KU ScholarWorks

Orientation dependence of heterogeneous nucleation at the Cu–Pb solid-liquid interface

Item Type	Article
Authors	Palafox-Hernandez, J. Pablo;Laird, Brian Bostian
Citation	Palafox-Hernandez, J. P., & Laird, B. B. (2016). Orientation dependence of heterogeneous nucleation at the Cu–Pb solid-liquid interface. The Journal of Chemical Physics, 145(21), 211914.
DOI	10.1063/1.4962424
Publisher	AIP Publishing
Rights	The following article appeared in TThe Journal of Chemical Physics 145, 211914 (2016); https://doi.org/10.1063/1.4962424 and may be found at http://doi.org/10.1063/1.4962424.
Download date	2024-08-01 01:31:45
Link to Item	http://hdl.handle.net/1808/25600

Orientation dependence of heterogeneous nucleation at the Cu–Pb solid-liquid interface

J. Pablo Palafox-Hernandez, and Brian B. Laird

Orientation dependence of heterogeneous nucleation at the Cu–Pb solid-liquid interface

J. Pablo Palafox-Hernandez[1] and Brian B. Laird[1,2,a)]

[1]*Department of Chemistry, University of Kansas, Lawrence, Kansas 66045, USA*
[2]*Freiburg Institute for Advanced Studies, Freiburg, Germany*

In this work, we examine the effect of surface structure on the heterogeneous nucleation of Pb crystals from the melt at a Cu substrate using molecular-dynamics (MD) simulation. In a previous work [Palafox-Hernandez *et al.*, Acta Mater. **59**, 3137 (2011)] studying the Cu/Pb solid-liquid interface with MD simulation, we observed that the structure of the Cu(111) and Cu(100) interfaces was significantly different at 625 K, just above the Pb melting temperature (618 K for the model). The Cu(100) interface exhibited significant surface alloying in the crystal plane in contact with the melt. In contrast, no surface alloying was seen at the Cu(111) interface; however, a prefreezing layer of crystalline Pb, 2-3 atomic planes thick and slightly compressed relative to bulk Pb crystal, was observed to form at the interface. We observe that at the Cu(111) interface the prefreezing layer is no longer present at 750 K, but surface alloying in the Cu(100) interface persists. In a series of undercooling MD simulations, heterogeneous nucleation of fcc Pb is observed at the Cu(111) interface within the simulation time (5 ns) at 592 K—a 26 K undercooling. Nucleation and growth at Cu(111) proceeded layerwise with a nearly planar critical nucleus. Quantitative analysis yielded heterogeneous nucleation barriers that are more than two orders of magnitude smaller than the predicted homogeneous nucleation barriers from classical nucleation theory. Nucleation was considerably more difficult on the Cu(100) surface-alloyed substrate. An undercooling of approximately 170 K was necessary to observe nucleation at this interface within the simulation time. From qualitative observation, the critical nucleus showed a contact angle with the Cu(100) surface of over 90°, indicating poor wetting of the Cu(100) surface by the nucleating phase, which according to classical heterogeneous nucleation theory provides an explanation of the large undercooling necessary to nucleate on the Cu(100) surface, relative to Cu(111), whose surface is more similar to the nucleating phase due to the presence of the prefreezing layer. *Published by AIP Publishing.* [http://dx.doi.org/10.1063/1.4962424]

I. INTRODUCTION

The most common mechanism for the formation of crystals from supercooled liquids is heterogeneous nucleation.[1] The presence of external surfaces (for example, the container or impurity particles) provides nucleation sites that typically lower the nucleation barrier below that associated with the corresponding process of direct homogeneous nucleation from the bulk fluid. Heterogeneous nucleation is a common phenomenon with tremendous implications in a number of fields including chemistry, physics, geology, materials science, and the pharmaceutical sciences. In a familiar example, it has been demonstrated that the formation of ice in clouds occurs by heterogeneous nucleation at impurity particles within cloud water droplets.[2] In another example from the pharmaceutical sciences, targeted heterogeneous nucleation has been used to control polymorphism in the crystallization of acetaminophen.[3] Despite its ubiquity, the understanding of heterogeneous nucleation, particularly, the mechanism by which substrate structure and composition influence the nucleation rates, is not well understood.

In a previous work, we examined the structure and transport properties of Cu(*s*)/Pb(*l*) interfaces as a function of the Cu substrate orientation [(111) or (100)] using molecular-dynamics (MD) simulation.[4] We found the interfacial structure of the two interfacial orientations to be qualitatively different. First, as observed previously by Webb *et al.*,[5] the surface of the Cu crystal at the (100) Cu(*s*)/Pb(*l*) was found to have a significant fraction of Pb atoms despite the fact that the solubility of Pb in crystalline Cu is negligible. In contrast to this surface alloying, the (111) interface exhibited 2-3 layers of crystalline Pb at the Cu surface. This "prefreezing" layer was found to have a lattice constant that was about 2% compressed relative to bulk fcc Pb and rotated by 6° relative to the underlying fcc Cu substrate. Unlike a true prefreezing layer, the thickness of this crystalline Pb layer did not diverge as the Pb melting point was approached from above, but instead remained 2-3 layers thick as the system is cooled below T_m for Pb. The large difference between these two surface structures provides a useful testbed to explore the effect of surface structure on the heterogeneous nucleation on chemically heterogeneous metal solid-liquid interfaces. In this work, we perform a series of MD simulations to examine the efficacy of heterogeneous nucleation of crystalline Pb at Cu (100) and (111) surfaces.

_____
a)Author to whom correspondence should be addressed. Electronic mail: blaird@ku.edu

There have been a number of atomistic simulation studies of the effect of surface structure on heterogeneous nucleation—see Refs. 6 and 1 for more complete reviews. One of the best studied model systems is that of hard-spheres at a wall. Courtemanche and van Swol[7] first reported that a prefreezing layer of (111) oriented fcc crystal forms at a structureless hard wall and that the width of this layer diverges as the freezing density of the fluid is approached from below. This phenomenon was confirmed in later much more detailed simulations by Dijkstra[8] and by later thermodynamic analyses.[9–11] The divergence of the width of the prefreezing layer would normally indicate that this nucleation barrier was zero (as may be expected for a surface phase exhibiting complete wetting); however, there has been shown to be a small, but significant contribution from line tension.[12–15] More recent studies by Winter et al.,[16] and Iwamatsu[17] highlight the relevance of line tension in the complete wetting scenario. Heni and Löwen[18] examined the hard-sphere fluid at a variety of static patterned hard walls with structures taken from various orientations of fcc and hcp lattices and reported strong surface structure dependence of the wetting of a hard-sphere crystal at these substrates.

Increasing in the complexity of the potential used, Wang et al.[19] studied the homogeneous and heterogeneous nucleation of Lennard-Jones (LJ) liquids. These authors used a substrate consisting of a 2-d hexagonal lattice of LJ particles to promote heterogeneous nucleation. The lattice constant of the substrate was varied relative to the LJ diameter (σ) to study the effect of lattice mismatch on heterogeneous nucleation. They reported an order of magnitude increase in the nucleation barrier for heterogeneous nucleation due to lattice mismatch of the substrate when the lattice constant of the substrate was decreased by 17% from that of the equilibrium bulk LJ solid. The effect of lattice mismatch was further discussed by Wang et al.[20] in a chemically heterogeneous metal-metal system [Al$_3$Ti(s)/Al(l)] using an Embedded Atom Model (EAM). In their study, various facets of Al$_3$Ti were used as substrates to nucleate liquid aluminum. In those nucleation experiments, the nucleation and crystal growth were observed to be significantly anisotropic. The (112) Al$_3$Ti interface nucleated at smaller undercooling than the (110) and (001) facets. The anisotropic behavior was attributed to the differences of interfacial free energies and the strain due to the lattice mismatch. However, there were still open questions regarding the role of the strain and lattice parameter mismatch.

All of these studies indicate that there is a strong dependence of surface structure on the kinetics (and thermodynamics) of heterogeneous nucleation of crystals from the melt. The strong anisotropy of the interfacial structure of Cu(s)/Pb(l) interfaces—surface alloying in the case of (100) and a prefreezing layer for (111)—makes this system ideal to extend the previous studies and expand our understanding of the effect of interfacial orientation and surface structure on heterogeneous nucleation. This paper is organized as follows: In Sec. II, we present a brief review of classical nucleation theory of heterogeneous nucleation, followed by a discussion of the simulation methodology and interface characterization protocols in Sections III and IV, respectively. Section V presents a review of our previous work[4] of the

interfacial structure of the Cu/Pb solid-liquid interface at 625 K (just above the Pb melting point) along with a new study of the changes induced in these interfaces at higher temperature (750 K). Finally, the main results examining the effect of interfacial orientation [(111) or (100)] on heterogeneous nucleation in this system are presented in Section VI.

II. CLASSICAL NUCLEATION THEORY AND HETEROGENEOUS NUCLEATION

The basic underlying physics of crystallization from the melt by homogeneous or heterogeneous nucleation can be understood through Classical Nucleation Theory (CNT),[21–25] in which the size of the nucleating cluster and the nucleation barrier are obtained from an examination of the balance between bulk free energy differences (which favor crystallization) and surface free energies, which oppose the formation of a nucleating cluster. In the CNT for homogeneous nucleation, the nucleating cluster is generally assumed to be a sphere of radius, R, leading to the following expression for the free energy of formation:

$$\Delta G_{\text{homo}} = \frac{4\pi R^3}{3} \rho_c \Delta\mu + 4\pi R^2 \gamma_{\text{sl}}, \quad (1)$$

where γ_{sl} is the solid-liquid interfacial free energy, ρ_c is the bulk crystal number density, and $\Delta\mu$ is the difference in the chemical potentials between the crystalline solid and liquid phases ($\Delta\mu = \mu_s - \mu_l$). Determining the maximum of ΔG_{homo} gives the following expression for the homogeneous nucleation barrier:

$$\Delta G^*_{\text{homo}} = \frac{16\pi}{3} \frac{\gamma^3_{\text{sl}}}{(\rho_c \Delta\mu)^2}. \quad (2)$$

For small undercoolings, $\Delta\mu \approx L\Delta T/T_m$, where L and T_m are the latent heat of fusion and melting point. This gives

$$\Delta G^*_{\text{homo}} = \frac{16\pi}{3L^2} \frac{T_m^2 \gamma^3_{\text{sl}}}{(\rho_c \Delta T)^2}. \quad (3)$$

For the fcc metals considered in this work, it has been shown that a hard-sphere based model works reasonably well and, to a good approximation, γ_{sl} is proportional to temperature[26]

$$\gamma_{\text{sl}} \approx 0.5 \rho_c^{-2/3} k_B T. \quad (4)$$

Substituting this into Eq. (3) gives

$$\Delta G^*_{\text{homo}} = \frac{2\pi k_B^3 T_m^2}{3L^2} \frac{T^3}{(\Delta T)^2}. \quad (5)$$

If one assumes that the rate, k, of nucleation is proportional to $\exp(-\Delta G^*/k_B T)$, we have

$$\Delta G^*_{\text{homo}}/k_B T = \frac{2\pi (k_B T_m)^2}{3L^2} \left(\frac{T}{\Delta T}\right)^2$$

$$= C^{\text{fcc}}_{\text{homo}} \left(\frac{T}{\Delta T}\right)^2, \quad (6)$$

where $C^{\text{fcc}}_{\text{homo}}$ is a constant and the fcc subscript is there to denote the fact that the equation was derived with the
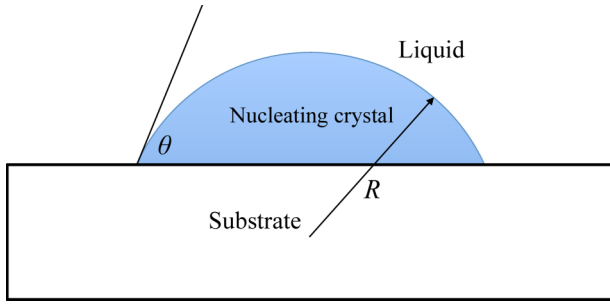
FIG. 1. Hemispherical cap geometry for classical heterogeneous nucleation theory.

assumption that the nucleating crystal is fcc. From simulation or experimental data, the value of $C_{\text{homo}}^{\text{fcc}}$ could be determined from plot of $\ln k$ versus $(T/\Delta T)^2$ and linear regression. A similar equation to Eq. (5) was also reported by Bokeloh, et al.[27] If one uses the fact that, for fcc forming materials, $L \approx k_B T$, then we predict that $C_{\text{homo}}^{\text{fcc}} \approx 2\pi/3 \approx 2.1$.

Despite its many approximations (e.g., assumption of spherical critical nucleus, applicability of macroscopic planar interface thermodynamics to highly curved nanoscale clusters), CNT provides an extremely useful, if not necessarily quantitative, theoretical framework within which to understand homogeneous nucleation,[28–30] and its predictions continue to be the subject of considerable experimental and computational studies. Building upon earlier work of Volmer,[31] an extension of CNT to heterogeneous nucleation was proposed by Turnbull.[32–34] In Turnbull's model, the nucleating cluster is assumed to be a hemispherical cap intersecting the substrate surface with a contact angle θ (see Fig. 1). The equation for the work required to form the nucleating cluster within CNT is

$$\Delta G_{\text{hetero}} = V(R,\theta)\Delta\mu + A_1(R,\theta)(\gamma_{\text{s,sub}} - \gamma_{\text{l,sub}}) + A_2(R,\theta)\gamma_{\text{sl}}, \tag{7}$$

where $V(R,\theta)$ is the volume of the cap, $A_1(R,\theta)$ and $A_2(R,\theta)$ are the areas of the cap-liquid and cap-substrate boundaries, respectively. The quantities $\gamma_{\text{s,sub}}$ and $\gamma_{\text{l,sub}}$ are the crystal-substrate and liquid-substrate interfacial free energies, respectively.

Using Young's equation for the contact angle,

$$\cos\theta = \frac{\gamma_{\text{l,sub}} - \gamma_{\text{s,sub}}}{\gamma_{\text{sl}}} \tag{8}$$

the heterogeneous nucleation barrier within Turnbull's CNT can be expressed as a fraction of the homogeneous nucleation barrier (Eq. (2)),

$$\Delta G_{\text{hetero}}^* = \Delta G_{\text{homo}}^* f(\theta). \tag{9}$$

In Eq. (9), the shape factor, $f(\theta)$, is given by

$$f(\theta) = (1 - \cos\theta)^2 (2 + \cos\theta)/4. \tag{10}$$

For heterogeneous nucleation then, Eq. (6) becomes

$$C_{\text{hetero}}^{\text{fcc}} = C_{\text{homo}}^{\text{fcc}} f(\theta). \tag{11}$$

From this analysis, the dependence of the heterogeneous nucleation rate on substrate surface structure depends upon

the degree to which the nucleating phase wets the substrate, as quantified by the wetting angle θ. As this wetting angle is decreased, a smaller nucleation barrier (and higher nucleation rate) is expected. The effect is substantial—a wetting angle of 30° corresponds to a value of $f(\theta)$ of 0.012, or a two-order of magnitude reduction in the nucleation barrier from the homogeneous value. In the Cu/Pb solid-liquid interface, there is a large difference in the interfacial structure depending upon the orientation of the Cu substrate. For Cu(100)/Pb, the substrate is a surface alloy (Pb/Cu) with an average lattice constant that close to that of crystalline Cu and significantly different than that of the nucleating Pb crystal. For the Cu(111)/Pb interface, the substrate upon which the liquid Pb would nucleate is the prefreezing layer, which has a 2-d hexagonal surface structure of Pb atoms, with a lattice constant that is about 2% smaller than that of a bulk Pb (111) crystal face. This lattice mismatch is expected to give rise to a non-zero nucleation barrier, but because this mismatch is small, we hypothesize that the nucleation barrier for (111) should be considerably smaller than that for the Cu(100)/Pb interface. Testing this hypothesis is the goal of this work.

III. SYSTEM AND SIMULATION DETAILS

In this work, we use an embedded atom model (EAM) for the Cu–Pb interatomic interactions developed by Hoyt et al.[35] This potential was used in our previous study of prefreezing in this system.[4] This potential has also been utilized in previous studies of the spreading of liquid Pb droplets on Cu surfaces[5] and the dynamics of Cu–Pb nanodroplets.[36] The melting temperatures for this model are 1279 K[35] (1357.8 K) and 618 K[4,37] (600.6 K) for Cu and Pb, respectively. The values in parentheses are the experimental melting points.[38]

The molecular-dynamics (MD) simulations discussed here were carried out using the parallel MD program LAMMPS[39] (Sandia Labs) with a time step of 1.0 fs. Both NVT and NPT simulations were used in this study. In addition, for the equilibration and data collection for systems containing a solid-liquid interface, NP_zAT MD simulations are used in which the interfacial area (A) is fixed and a barostat is applied to enforce constant pressure normal to the interfacial plane. Temperature was regulated in each simulation using a Nosé-Hoover thermostat,[40] with a thermostat relaxation time of 0.1 ps. For the constant-pressure simulations, an Anderson piston barostat is employed with a relaxation time constant of 1.0 ps. Periodic boundary conditions are applied in all Cartesian directions.

For the simulations at $T = 625$ K and below, complete compositional segregation between the coexisting solid (Cu) and liquid (Pb) phases is assumed, based on the experimental phase diagram, which shows only negligible solubility of Cu in liquid Pb and of Pb in crystalline Cu. The validity of this assumption is supported by the fact that the MD simulations of Cu/Pb solid-liquid interfaces were compositionally stable for both interfacial orientations studied: (100) and (111). However, the assumption of mutual
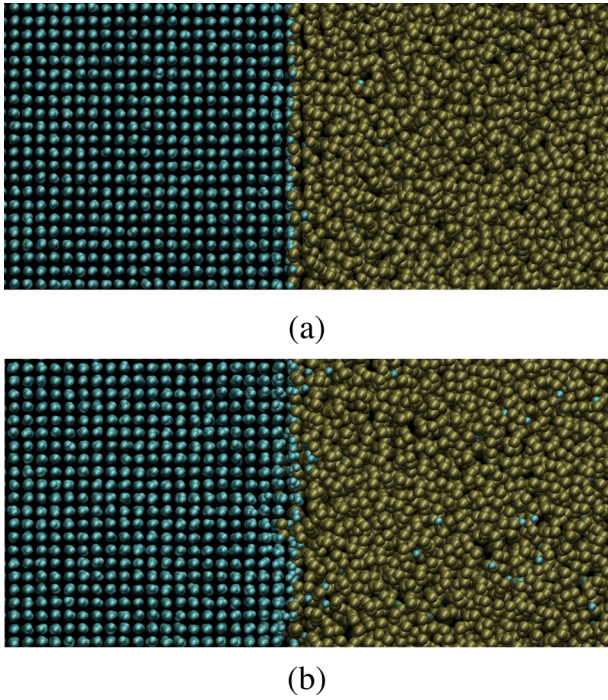
FIG. 2. Snapshot of Cu–Pb (100) solid-liquid interface at 625 K (a), and 750 K (b).

FIG. 3. Snapshot of Cu–Pb (111) solid liquid interface at 625 K (a), and 750 K (b).

immiscibility was not found to be appropriate for the higher-temperature simulations at $T = 750$ K because simulations so constructed are compositionally unstable over the course of a few nanoseconds, with a significant number of Cu atoms dissolving into the liquid phase. To remedy this, the equilibrium concentration of Cu in the liquid phase was determined by constructing a Cu(100)/Pb(l) interface and evolving using NP_zAT MD at 750 K until the Cu mole fraction in the bulk liquid reached a saturation equilibrium value, which was found to be $x_{Cu}^l = 0.027(1)$ after a 34.5 ns run. Using this value for x_{Cu}^l, together with the assumption of negligible solubility of Pb in crystalline Cu (supported by the phase diagram), the solid-liquid interfaces at 750 K remained compositionally stable over the length of the simulations performed.

The equilibrated interfacial systems studied here were created as follows: For the (100) interfacial orientation, a sample of bulk Cu crystal was prepared with 15 360 atoms ($32 \times 32 \times 15$ unit cells). Meanwhile, the (111)-oriented crystals had 18 144 atoms ($24 \times 14 \times 9$ unit cells). Each crystal sample was equilibrated at the desired temperatures using NPT simulations. For the liquid phase, 12 000 Pb liquid atoms were equilibrated using NP_zAT MD, with the area (A) fixed to equal the area of the equilibrium crystal sample for each interfacial orientation and temperature studied. After equilibration, in the systems at 750 K, the corresponding number of Pb atoms are exchanged for Cu atoms to fulfill the liquid equilibrium composition previously calculated, $x_{Cu}^L = 0.027(1)$. The interfacial systems were assembled and equilibrated from the bulk samples using the protocol outlined in Ref. 4. Figs. 2 and 3 show snapshots from the equilibrium simulations at 625 K and 750 K, respectively.
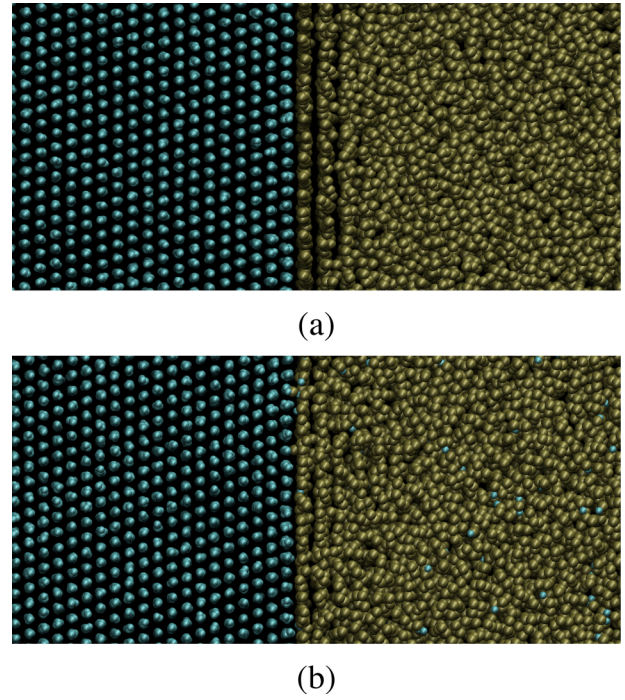
IV. INTERFACE CHARACTERIZATION

The properties of the interface are characterized by measuring property-specific interfacial profiles - that is, plots of variation of selected properties as a function of z, the direction normal to the interfacial plane. Two kinds of interfacial profiles are used: fine-scale and coarse-grained. The fine-scale profiles are calculated by dividing the length of the box in the z direction in bins and averaging the property of interest within that bin. On the other hand, the coarse-grained profiles are computed by applying a finite response filter (FIR) to the fine-scale profiles. For the full description of this technique the reader is referred to Refs. 4 and 41–43. The fine-scale profiles are defined as follows:

- *Density profiles:* $\rho_i(z)$ (i = Cu or Pb) for each atom type is given by

$$\rho_i(z) = \frac{\langle N_z^i \rangle}{A_{xy}\Delta_z}, \qquad (12)$$

  where Δ_z is the bin spacing, $\langle N_z^i \rangle$ is the average number of atoms of type i in the bin defined by $z - \Delta_z/2 < z < z + \Delta_z/2$ and A_{xy} is the interfacial area.

- *2-dimensional Single-particle Densities:* $\langle \rho_{xy}(\vec{r}) \rangle$ for the first two Cu layers and first two Pb layers at the interface, as well as Cu and Pb layers in the bulk solid and liquid (i.e., far from the interface), respectively. These calculations were performed for (111) interface orientations. Each plane was divided in 225 bins in the x direction and 384 bins in the y, and the average position of the atoms involved is calculated over 2 ns from the recorded positions taken every 1 ps.

- *Structure factor:* The 2-d structure factor[44] is defined as

$$F_{xy}(\vec{k}) = \langle |\rho_{xy}(\vec{k})|^2 \rangle, \qquad (13)$$

where $\rho_{xy}(\vec{k})$ is the Fourier transform of the 2-d instantaneous particle density $\rho_{xy}(\vec{r})$. To calculate $F_{xy}(\vec{k})$ instantaneous structure factors were calculated from configurations recorded every 1 ps (1000 time steps) and averaged over the final 2 ns of the simulation run.

- *Stress profile:* $S(z)$, the stress along the normal direction to the interface is determined from the components of the pressure tensor, P_{ij},

$$S(z) = P_{zz} - \frac{1}{2}[P_{xx}(z) + P_{yy}(z)]. \qquad (14)$$

$S(z)$ measures the difference between the longitudinal and transverse diagonal components of the pressure (stress) tensor. The calculation of the stress profile in a simulation requires the calculation of the local stress tensor associated with individual atomic positions. For this calculation, we use the procedure implemented in LAMMPS.[45]

For a solid-liquid interface under hydrostatic stress, $S(z)$ should be zero away from the interfacial region, as the tangential and normal components of the stress tensor should be equal in a bulk system. However, due to excess interfacial stress, the tangential component will differ from the bulk value in the interfacial region. It is especially critical to monitor in the bulk solid, as residual stress in this region is an indication of a faulty interface equilibration protocol.

- *Diffusion profile*: To calculate the diffusion profile, we utilize bins along the z direction defined as the regions between the minima of the density profile. For each of these bins, we calculate the average mean-square displacement (MSD) per particle, $\langle |\mathbf{r}_j(t) - \mathbf{r}_j(t_0)|^2 \rangle_z$, for particles initially in the bin centered at z at time $t = 0$. In addition to averaging over all atoms in each bin, we also average over 50 time origins separated by 0.5 ps (500 time steps). Once the MSD is calculated as a function of time, the diffusion constant is determined from the limiting slope of the MSD versus time plot

$$D(z) = \frac{1}{6}\frac{d}{dt}\langle [\mathbf{r}_j(t) - \mathbf{r}_j(t_0)]^2 \rangle_z. \qquad (15)$$

In addition to characterization of the equilibrium interface, we aim to characterize the kinetics of heterogeneous nucleation of crystalline Pb on the Cu substrate as the system is cooled below the Pb melting point. The degree of Pb crystallinity in the system is quantified by the 2-d order parameter q_6 implemented by Davidchack and Laird.[42] The q_6 order parameter properly characterizes hexagonal crystalline patterns such as the one observed in the Pb prefreezing layer. The q_6 parameter is defined as

$$q_6(z) = \left\langle \frac{1}{N}\sum_{i,j,k} \cos[6\theta_{xy}(i,j,k)] \right\rangle \qquad (16)$$

here the sum over i, j, k represents the angle formed by the nearest neighbors in the same bin, θ_{xy} is the angle between r_{ij} and r_{ik} projected in the xy plane. This parameter varies from nearly 0 for a liquid to 1 for a perfect FCC crystal.

The variation of the order parameter q_6 in the z direction is used to determine the position of the interface. The position of each interface is calculated by fitting the q_6 values (of a given snapshot) to a hyperbolic tangent[46]

$$f(z) = a + b\tanh\,[z - C_{\text{pos}}]/d, \qquad (17)$$

here a, b, C_{pos}, and d are fitting parameters, from these, the C_{pos} parameter is predicting the position of the interface.

The change of the interface position as a function of time is used to track the nucleation and growth in undercooling simulations. Once the nucleation occurs for a given system, the interface position is fit to a line. From the linear regression the nucleation time is estimated. Given that nucleation is a random event, performing a large number of simulations will yield the probability distribution for a given undercooling temperature. These nucleation-times probability distributions are treated with the experimental methodology developed by Haymet and collaborators[47–49] to estimate the nucleation rates. Once the nucleation distributions are obtained, the unfrozen fraction, $F(t)$, at time t is computed by

$$F(t) = \frac{N(t)}{N_0}, \qquad (18)$$

where N_0 is the total number of simulations (samples), and $N(t)$ is the number of unfrozen simulations at time t. These decay curves are used to describe the kinetics of freezing. However, the interpretation of these results requires the specification of a plausible mechanism that properly describes the kinetics. As a first step, we assumed a first order kinetics where the liquid phase A becomes the crystalline phase B as

$$A \xrightarrow{k} B. \qquad (19)$$

First-order kinetics and the decay curves are related by

$$F(t) = \frac{N(t)}{N_0} = e^{-kt}. \qquad (20)$$

Therefore the rate constant k can be obtained from a plot of $\ln\,[F(t)]$ versus t. In this case the kinetic constant is the nucleation rate, assuming that the proposed mechanism is correct.

V. INTERFACE COMPARISON AT 625 K AND 750 K

In our previous work,[4] we reported a detailed comparison of the structure and transport properties of the (111) and (100) Cu(s)/Pb(l) interfaces at 625 K, just above the melting point of Pb. Here we expand that work to examine temperature-dependent changes in interfacial structure as the system is heated from 625 K to 750 K. The density profiles for the (100) and (111) crystal orientations are shown in Figs. 4 and 5, respectively. Although, the density profiles at the two temperatures are very similar, there are small qualitative differences related to composition. First, in both interfacial
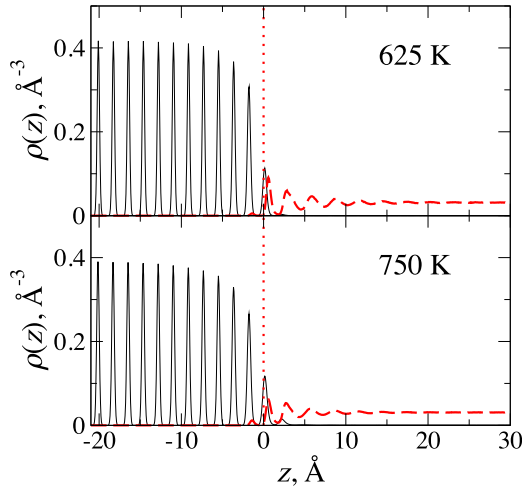
FIG. 4. Density profiles for the (100) interface at 625 K (top) and 750 K (bottom), for Cu (black) and Pb (red). The position of the dividing surface ($z = 0$, dotted vertical line) is chosen such that the interfacial excess of Cu atoms is zero.

orientations at 750 K, there is a small amount of Cu in the first layer of liquid Pb near the interface that was not present at 625 K. This indicates an interface-induced enhanced solubility of Cu in the Pb liquid near the Cu surface. There is significant and continual exchange of material between this first liquid layer and the surrounding layers, so we are confident that we are measuring a compositionally equilibrated interface. Second, there is a small increase in the fraction of lead in the second Cu layer from the interfacial plane surface alloy in the second crystal layer of the (100) crystal—see Fig. 4.

More significant differences are observed in the stress at the two temperatures (see Fig. 7). In both interfaces—(100) and (111)— the intensity and depth of the peaks in the stress profiles decreases significantly when the temperature is increased. In the case of the (100) interface the changes are only quantitative—the overall shape of the profile remains the same. However, for the (111) interface, the pronounced double peak observed at 625 K in the stress profile becomes a single
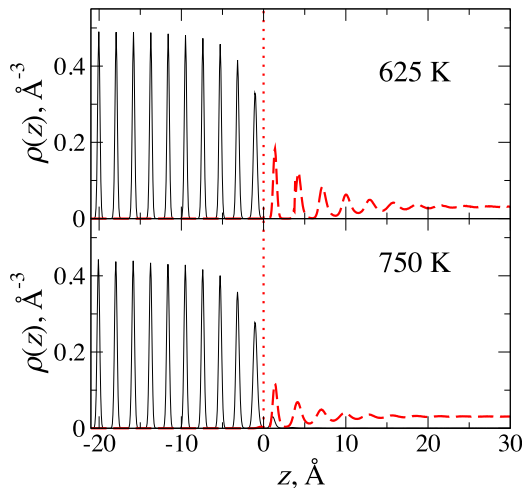
TABLE I. Excess interfacial properties of the Cu(s)/Pb(l) interface in units of J m^{-2}.

Orientation	$T(K)$	τ (J m^{-2})	e (J m^{-2})
(100)	625	−0.135(2)	−0.363(5)
(100)	750	−0.06(1)	−0.263(4)
(111)	625	−0.44(3)	−0.252(2)
(111)	750	−0.21(3)	−0.362(4)

peak (with a shoulder) at 750 K. This variation is strongly correlated with the structural changes taking place due to the temperature increment, the correlation will be clear when the 2-D density and structure profiles are discussed. Additionally, the total excess interfacial stress [which is the integral of $S(z)$] and the excess interfacial energy were calculated, the results can be seen in Table I. The excess stresses, τ, at 725 K for the (111) and (100) interfaces are −0.21(3) and −0.06(1) J m^{-2}, respectively, indicating that like the interfaces at 625 K, the interfaces at 750 K are under compression, although the magnitude of the stress is lower at the higher temperature. The excess energies (based on a Gibbs dividing surface with zero excess interfacial Cu) are all negative, increasing (becoming less negative) with temperature for (100), but decreasing for (111).

The qualitative change in the stress profile for the (111) interface is an indicator of structural changes taking place
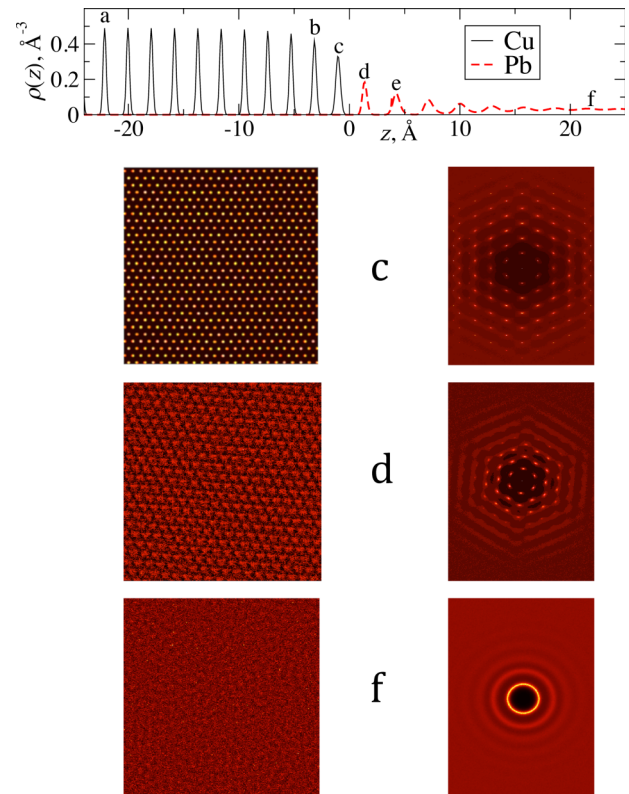

FIG. 6. 2-D densities (left) and Fourier structure factors (right) for the layers adjacent to the Cu(111)/Pb interfacial plane at 625 K: ((c) and (d)) the first Cu and Pb planes adjacent to the interface, (f) a plane deep into the Pb liquid bulk the position of these planes is illustrated in the density profile reproduced at the top of the figure.
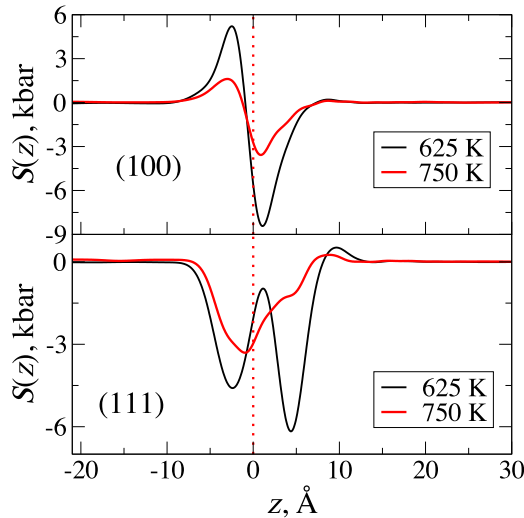

FIG. 5. Density profiles for the (111) interface at 625 K (top) and 750 K (bottom), for Cu (black) and Pb (red). The position of the dividing surface ($z = 0$) is chosen such that the interfacial excess of Cu atoms is zero.

FIG. 7. Stress profiles at 625 K and 750 K for the (100) (top) and (111) (bottom) interfaces. The position of the diving surface ($z = 0$) is chosen such that the interfacial excess of Cu atoms is zero.

as temperature is increased. To examine this more closely, we perform an analysis of the 2-d structure of the interfacial layers adjacent to the (111) interfaces. Fig. 6 shows the 2-d real- and Fourier-space single particle densities for several planes near the (111) interface, as well as for the bulk. These data were previously reported in our earlier paper[4] to show the existence of a crystalline Pb slab (2-3 atomic layers

thick) between the Cu substrate and the Pb liquid. These hexagonal Pb crystalline layers are rotated 6° relative to the underlying (111) Cu substrate and have a lattice constant that is slightly compressed ($\approx 2\%$) relative to bulk fcc Pb. The hexagonal structure and the 6° rotation can be clearly seen in the 2-d Fourier structure factor plot for layer d in Fig. 6 at 625 K—note the Bragg peak spacing in "d" (the first Pb layer) is much smaller than that in layer "c" (the first Cu solid layer) consistent with the much larger lattice constant for Pb, relative to Cu. This structure accounts for the double peak in the stress profile for the (111) interface at 625 K (Fig. 7)—the first peak corresponding to a Cu(s)/Pb(s) interface and the second to the Pb(s)/Pb(l) interface. Fig. 8 shows the corresponding structural data at the higher temperature—750 K. The structure of first interfacial Cu(s) layer (layer "c" in the plots) changes relatively little from 625 K to 750 K. At 750 K, the Pb crystalline structure in the first Pb layer ("d") is gone—the faint Bragg peaks seen in layer "d" at 750 K correspond to Cu crystalline "islands" due to the rougher Cu surface at the higher temperature. Thus, the prefreezing structure seen at 625 K in the (111) interface is not present at 750 K.

To determine mobility within the interface, we have calculated self-diffusion profiles—shown in Figs. 9(a) and 9(b) for both 625 K and 750 K. As expected, the Pb diffusion constants are significantly higher in the bulk and at the
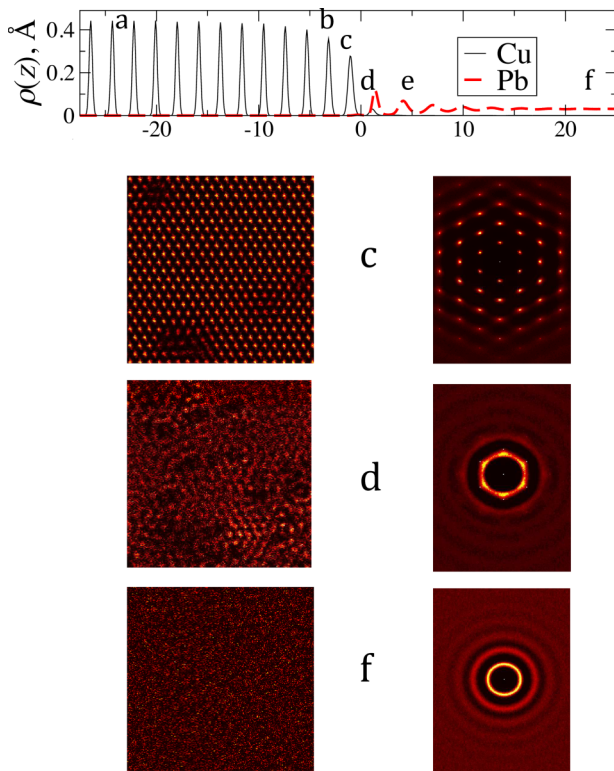

FIG. 8. 2-D densities (left) and Fourier structure factors (right) for the layers adjacent to the Cu(111)/Pb interfacial plane at 750 K: ((c) and (d)) the first Cu and Pb planes adjacent to the interface, (f) a plane deep into the Pb liquid bulk the position of these planes is illustrated in the density profile reproduced at the top of the figure.
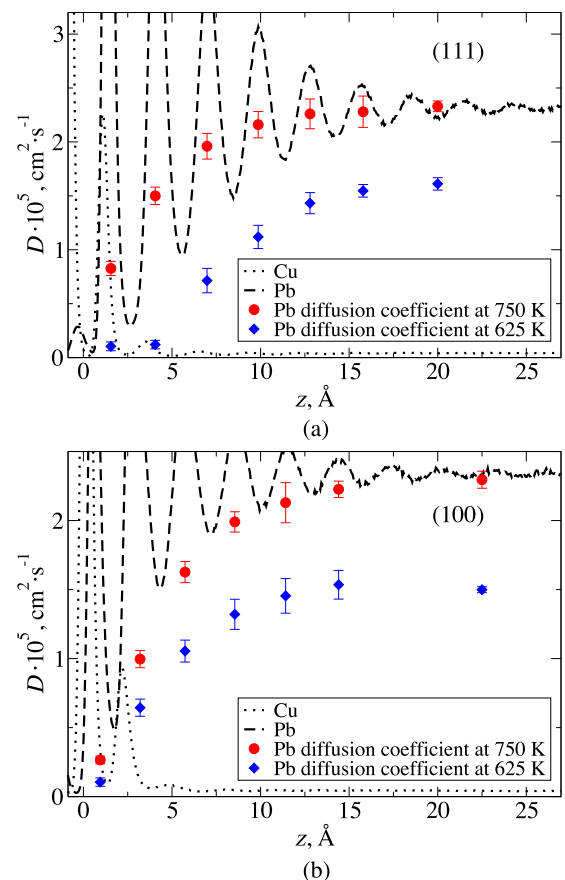

FIG. 9. Diffusion coefficient profiles for the (111) (top) and (100) (bottom) Cu–Pb interface at 625 K and 750 K. For ease of comparison, the corresponding Cu and Pb density profiles at 750 K are shown.

interface at 750 K than at 625 K. However, for (111) there is a qualitative change in the shape of the diffusion curve in going from 625 K to 750 K. At 625 K, the diffusion constant of the first two lead layers is very close to zero, consistent with the solid prefreezing layer. At 750 K, there is an order of magnitude increase in D in the second Pb layer, consistent with the structural analysis that this is now a liquid-like layer, in contrast to the prefreezing layer seen at 625 K.

VI. ORIENTATION DEPENDENCE OF HETEROGENEOUS NUCLEATION

The data in Sec. V show that the prefreezing solid-Pb layer seen at the Cu(111)/Pb(l) solid-liquid interface vanishes as the temperature is raised sufficiently. This is consistent with typical prefreezing or premelting behavior. However, as discussed in our previous work,[4] one major difference in the prefreezing behavior seen in the Cu(111)/Pb(l) interface is the fact that the width of the prefreezing layer does not diverge as the melting point is approached from above, as is the case in other systems, such as hard spheres.[8] Such a divergence indicates that the growth of the prefreezing crystal at the surface is barrier-less—or at least nearly so.[14] In the case of the Cu(111)/Pb, however, the fact that the width of the prefreezing layer does not increase much beyond 2-3 lattice planes, even as the temperature is lowered below the melting point for this model (618 K), indicates there is a significant barrier to nucleation of a bulk Pb crystal. In our previous work[4] we noted that this was likely due to the fact that the prefreezing layer had a slightly smaller lattice constant (by 2%) than bulk crystalline Pb. The free energy necessary to overcome the stresses induced by the lattice mismatch would give rise to a significant nucleation barrier.

Two types of interfacial structures were observed above the lead melting point at 625 K: prefreezing for the Cu(111) orientation and surface alloying for Cu(100).[4] In this section, we examine the qualitative and quantitative effect of interfacial orientation on the heterogeneous nucleation of Pb crystals at the Cu/Pb solid-liquid interface. Specifically, we determine efficacy of both the prefreezing layer for Cu(111)/Pb(l) and the surface alloyed solid layer in Cu(100)/Pb(l) as seed surface for heterogeneous nucleation of crystalline Pb. In Subsection VI A, which follows, we use crystallinity order parameters to monitor the nucleation and growth of crystalline Pb on the Cu(111) interface and give an estimate of the nucleation barrier. In Subsection VI B, we examine qualitatively the nucleation and growth of crystalline Pb on the surface allowed interface of Cu(100)/Pb(l). The major conclusion is that the presence of the prefreezing layer on Cu(111) significantly enhances heterogeneous nucleation relative to Cu(100).

A. Heterogeneous Nucleation at a Cu(111)/Pb(l) Interface

A large set of MD simulations were performed to investigate the impact of the $(6 \times 6)R6°$ prefreezing layer

(a) 0.0 ns

(b) 0.95 ns

(c) 1.25 ns
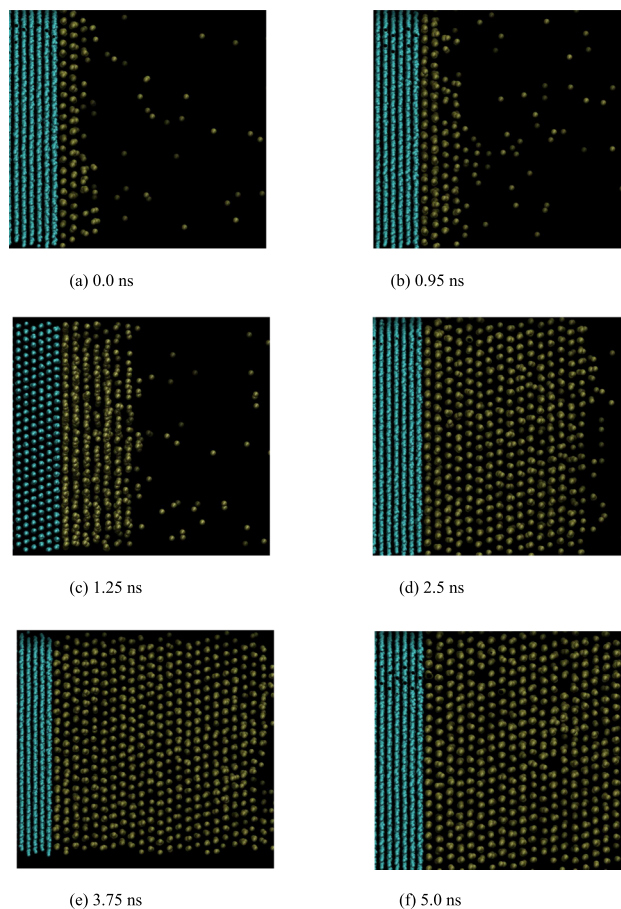
(d) 2.5 ns

(e) 3.75 ns

(f) 5.0 ns

FIG. 10. Cu(111)-Pb interface at 592 K nucleating and growing. The atoms with an order parameter lower than 0.8 were removed to better depict the crystal growth.

at the Cu(111)/Pb solid-liquid interface on heterogeneous nucleation. To first qualitatively determine a temperature range over which heterogeneous nucleation can be observed in this system, we start with a configuration equilibrated at 625 K, just above the melting point of Pb. A series of 5 ns $NPAT$ simulations were then run at successively lower target temperatures (in decrements of 5 K), and the configurations were recorded. Heterogeneous nucleation was observed in these test runs between 595 K and 590 K. Within this range, further simulations were carried out in decrements of 1 K. It was found that at 592 K both interfaces of the system (left and right) nucleated within the 5 ns time scale. For this temperature, Fig. 10 shows a series of snapshots between 0 and 5.0 ns to follow the nucleation and subsequent crystal growth in this system by monitoring the q_6 order parameter (discussed in Section IV) to distinguish between crystalline and liquid Pb atoms. In Fig. 10, only the crystalline Cu and Pb atoms are shown and the nucleation and growth are shown to occur primarily layer-wise, without the formation of the hemispherical cap that is often assumed in a heterogeneous nucleation mechanism—although it is possible that the contact angle is small enough that it appears of the size of current system to be approximately constant. To construct Fig. 10, we define all atoms with a value of q_6 greater than 0.8 as being crystalline. Fig. 11 shows the distribution of order parameter
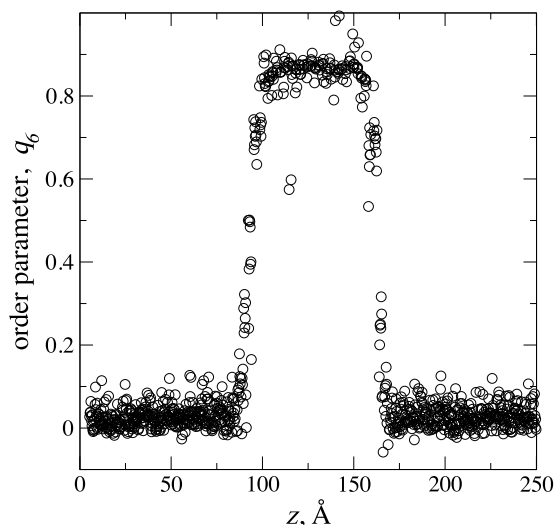
FIG. 11. Order parameter taken from the starting configuration at 592 K. The values closer to one correspond to the crystal phase, and the values closer to zero to the liquid phase.

FIG. 13. Decay curves showing the unfrozen fraction $F(t)$ for different temperatures.

values in the starting configuration of the 592 K run (before nucleation).

In these simulations, the cross-sectional dimensions of the simulation box parallel to the interfacial plane are determined by the Cu lattice constant. Because the lattice constant of the Pb prefreezing layer is substantially different than that of Cu and the Pb layer is rotated by 6° relative to the Cu lattice, there is a possibility of substantial system size effects. In our previous work,[4] we demonstrated that quadrupling the cross-sectional area did not change the results for the interfacial properties studied—although decreasing it by a factor of four did have a substantial effect.

To quantify the heterogeneous nucleation, we create 50 starting configurations chosen from an MD run at 600 K by taking samples every 50 ps. Each of these starting configurations is then quenched over 0.5 ns to a target undercooling temperature. We choose several target
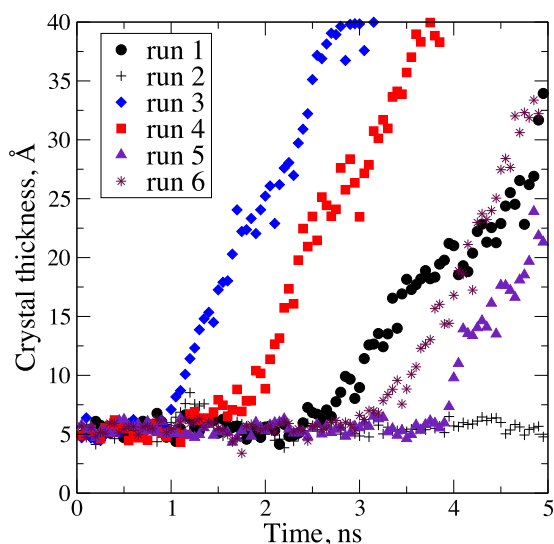
temperatures to examine the temperature dependence of the nucleation rate: 592 K, 590 K, 588.5 K, and 587 K. After reaching the target temperature, the system is monitored for another 4.5 to 9.5 ns, depending on the system. The position of the Pb(s)/Pb(l) interface, as determined from the q_6 order parameter profile, is then used to determine a Pb crystal thickness as a function of time, which is then plotted for each system. Fig. 12 shows examples of such plots for several independent runs at 592 K. Once the thickness of the Pb crystal as a function of time is found, a linear regression is performed to calculate the nucleation time for each interface (left and right) of all the simulations. Because there are two interfaces in each simulation, the data consist of nucleation times for 100 independent interfaces. The nucleation rate is determined by calculating the fraction $F(t)$ of systems that have not nucleated within time t—see Eq. (18), which are then fit assuming first-order kinetics using Eq. (20) to determine the nucleation rate, k. The unfrozen fraction $F(t)$ for the various temperatures studied is plotted in Fig. 13. Fig. 14

FIG. 12. Pb crystal thickness over time for several (111) nucleation simulations at 592 K.
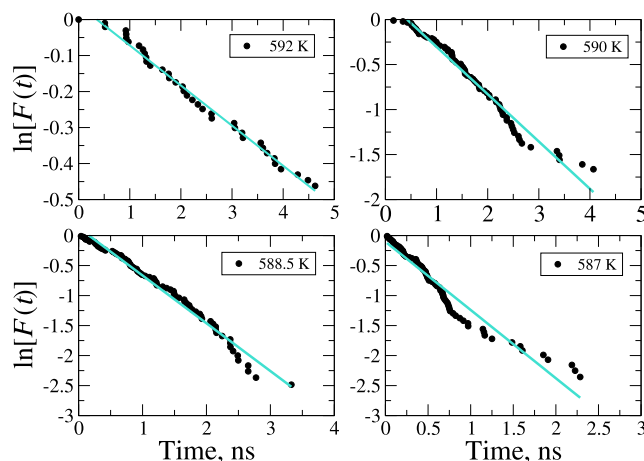

FIG. 14. Log-linear plots of $F(t)$ at various temperatures, from the slope of these curves a nucleation rate k is estimated.
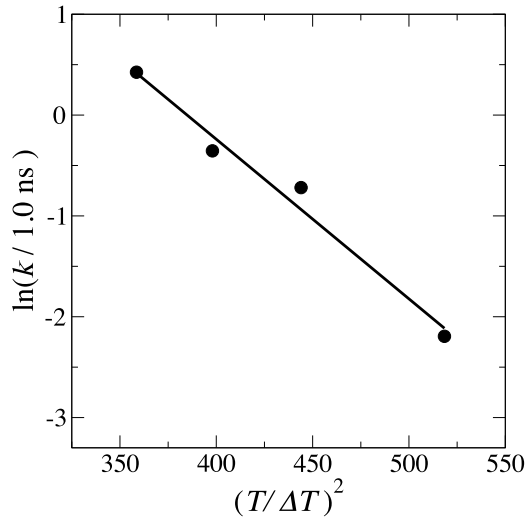
FIG. 15. Log-linear plot of the nucleation rates versus $(T/\Delta T)^2$ to determine the constant $C_{\text{hetero}}^{\text{fcc}}$.

shows the log-linear plot used to calculate the nucleation rates at each temperature. We have tested and determined that the results here are not very sensitive—at least within the simulation errors—to the exact time range over which the linear regression is performed.

Assuming Eq. (6) is valid, we plot the nucleation rates in a log-linear plot versus $(T/\Delta T)^2$ and do a linear regression to find $C_{\text{hetero}}^{\text{fcc}}$. This plot is shown in Fig. 15. For this system the value of $C_{\text{hetero}}^{\text{fcc}}$ was found to be 0.016(2), which as expected is considerably smaller than the value predicted for homogeneous nucleation using CMT. From Eq. (11), this would imply a contact angle of 26°. Our observed value is likely somewhat smaller than that given the size of our system, but given the approximations of CNT, this is a reasonable result.

From these data, we see that, even though the substrate at this interface is a prefreezing layer consisting of a 2-d hexagonal lattice of Pb atoms, the small lattice mismatch (2%) of this layer with the nucleating crystal gives rise to a nucleation barrier large enough that no nucleation is seen in our simulations below a 26 K undercooling. This finding is consistent with previous simulation results on the heterogeneous nucleation of a LJ fluid at a LJ lattice[19] and of Al on Al$_3$Ti[20] that observe a significant decrease in the rate of heterogeneous nucleation with increasing lattice mismatch.

B. Cu(100)/Pb(*l*) interface

Cooling experiments to observe heterogeneous nucleation were also performed as well on the Cu(100)/Pb interface. First, a NP_zAT simulation at 545 K showed no signs of crystallization over a run of 65.5 ns. Given this result a configuration from this simulation was taken and cooled down further to 450 K and run at $NPAT$. In this system, nucleation of a Pb crystal was observed at this temperature after 10.15 ns. A series of snapshots from this run are presented in Fig. 16 to illustrate the evolution of the critical nucleus and subsequent crystal growth. In this crystal orientation, the

(a) 10.15 ns

(b)10.20 ns
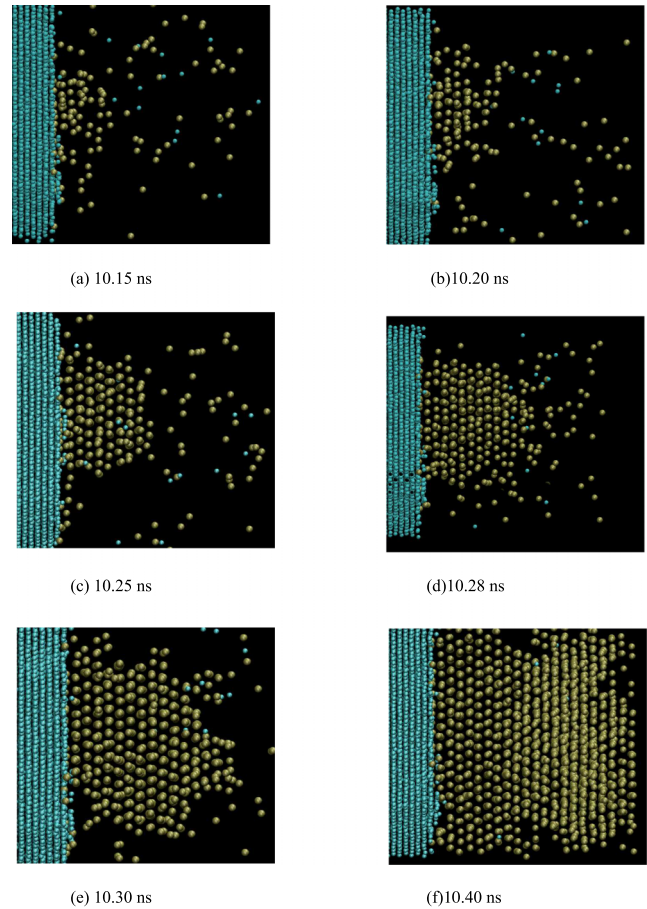
(c) 10.25 ns

(d)10.28 ns

(e) 10.30 ns

(f)10.40 ns

FIG. 16. Snapshots from the Cu(100)/Pb interface at 450 K illustrating the crystal formation. The atoms with an order parameter lower than 0.8 were removed to better depict the crystal growth.

critical nucleus is observed to be a hemispherical cap of fcc Pb at the Cu(100) surface. The contact angle for the Pb crystal at the surface is observed to be large (>90°), although our statistics are not sufficient to get an accurate value. This indicates that the wetting of the Cu(100) surface by the Pb crystal is relatively poor. The elapsed time from the nucleation of the cap until the crystal growth layer wise is approximately 0.15 ns—the driving force for solidification is quite large at this temperature, so that once the critical nucleus is reached, crystallization was rapid. According to Eq. (9) the large contact angle of the nucleating phase on the Cu(100) surface relative to that for the (111) surface, for which nearly complete wetting is observed, is consistent with the fact that nucleation on the simulation time scale on the (100) surface only takes place at a much lower temperature [450 K versus 590 K for (111)].

As for the Cu(111) interface, we performed a series of cooling simulations for several temperatures around 450 K. However, this system did not lend itself well to quantitative analysis. Because the crystal nucleation was not approximately planar [as it was for (111)] and the subsequent crystal growth was very rapid, our automated protocols for determining nucleation times did not work well and visual inspection was necessary to determine nucleation times for each run. After analysis, our statistics were poor for this system and we

were unable to get quantitative nucleation rate constants; but qualitatively our observations indicate that

(a) The rates of heterogeneous nucleation of Pb crystal on Cu(100) are orders of magnitude slower than that on Cu(111) given that an undercooling of about 170 K is necessary for nucleation on Cu(100) to be observed—relative to about 25 K for (111).

(b) The higher nucleation barrier for Pb solidification on Cu(100), relative to that on Cu(111), is likely due primarily to the poor wetting of the Cu(100) surface by the Pb crystal, relative to that for Cu(111).

VII. SUMMARY

In this work, we have examined the effect of surface structure and orientation on the heterogeneous nucleation of crystalline Pb from the melt at a Cu substrate. Near the melting point of Pb (618 K for the model used here), significant differences have been observed in molecular-dynamics (MD) simulations between the interfacial structures of the Cu(111)/Pb and Cu(100)/Pb solid-liquid interfaces,[4] providing an ideal system for this study. The Cu(100)/Pb solid-liquid interface exhibits marked surface alloying of the crystal plane in contact with the Pb liquid, but with a lattice constant that is close to the bulk Cu fcc value. There is no surface alloying observed in Cu(111), in contrast. Instead, a prefreezing slab forms at the surface consisting of 2-3 2-d hexagonal Pb crystal planes rotated about 6° relative to the underlying Cu(111) substrate. The lattice constant of this prefreezing layer is about 2% compressed relative to bulk Pb crystal, yielding a small lattice mismatch that could potentially have an effect on heterogeneous nucleation.

Our earlier work[4] examined only the interfaces at 625 K. To study this in more detail, we have characterized the interfaces at a higher temperature of 750 K. We observe that the surface alloying of Cu(100) persists at the higher temperature; however, the prefreezing layer in Cu(111) is no longer observed. In other studies of prefreezing,[8] the thickness of the layer diverges as the freezing point is approached from above; however, in the case of Cu(111)/Pb, the prefreezing layer, although it vanishes at high temperature, remains finite in thickness as the system is cooled to T_m(Pb) and below, indicating that there is a significant barrier to nucleation of fcc Pb crystal on this surface.

By examining the results of a number of MD simulations in which the system is systematically cooled below the melting point of lead (618 K for the model used), we observe significant differences in the ability of the Cu surface to nucleate crystalline Pb as a function of interfacial orientation (and structure). For the Cu(111) system, heterogeneous nucleation is observed within the simulation time at 592 K, which corresponds to an undercooling of 26 K. The critical nucleus was nearly planar and the subsequent crystal growth proceeded layer-wise. Classical heterogeneous nucleation theory[32–34] predicts that the heterogeneous nucleation barrier is reduced significantly from the corresponding barrier for homogeneous nucleation by a factor $f(\theta)$ which depends upon

the wetting contact angle θ of the nucleating phase on the substrate. We have estimated the heterogeneous nucleation rate constants for the Cu(111)/Pb interface at several temperatures near 592 K. Fitting these to the predictions of classical heterogeneous nucleation theory yields a nucleation barrier that is two orders of magnitude smaller than the predicted value for homogeneous nucleation—consistent with a very small contact angle for the nucleating Pb crystalline phase.

In contrast, heterogeneous nucleation on the Cu(100) surface was observed to be considerably less favorable than for Cu(111). To observe nucleation on a reasonable simulation time (10 ns) an undercooling of approximately 170 K was necessary (450 K)—in contrast to the 26 K undercooling required for Cu(111). Snapshots from the nucleating system show that the critical nucleus—instead of being nearly planar as observed for Cu(111)—was a hemispherical cap with a contact angle with the surface of greater than 90°, which is an indication that the nucleating phase (Pb crystal) poorly wets the Cu(100) surface. Thus, our results are consistent with the classical nucleation theory prediction that the degree to which the nucleating phase wets the substrate is the major factor in determining the barrier to nucleation—relative to the homogeneous process. Note that, even though we observe a high heterogeneous nucleation barrier for the Cu(100) surface, it is still lower than that for homogeneous nucleation, which was never observed to occur in the simulations.

[1]G. C. Sosso, J. Chen, S. J. Cox, M. Fitzner, P. Pedevilla, A. Zen, and A. Michaelides, Chem. Rev. **116**, 7078–7116 (2016).

[2]B. J. Murray, D. O'Sullivan, J. D. Atkinson, and M. E. Webb, Chem. Soc. Rev. **41**, 6519–6554 (2012).

[3]K. Chadwick, A. Myerson, and B. Trout, CrystEngComm **13**, 6625–6627 (2011).

[4]J. P. Palafox-Hernandez, B. B. Laird, and M. Asta, Acta Mater. **59**, 3137–3144 (2011).

[5]E. B. Webb III, G. S. Grest, and D. R. Heine, Phys. Rev. Lett. **91**, 236102:1–4 (2003).

[6]J. Anwar and D. Zahn, Angew. Chem., Int. Ed. **50**, 1996–2013 (2011).

[7]D. J. Courtemanche and F. van Swol, Phys. Rev. Lett. **69**, 2078–2081 (1992).

[8]M. Dijkstra, Phys. Rev. Lett. **93**, 108303 (2004).

[9]M. Heni and H. Löwen, Phys. Rev. E **60**, 7057–7065 (1999).

[10]B. B. Laird and R. L. Davidchack, J. Phys. Chem. C **111**, 15952–15956 (2007).

[11]B. B. Laird and R. L. Davidchack, J. Chem. Phys. **132**, 204101 (2010).

[12]S. Auer and D. Frenkel, Nature **409**, 1020–1023 (2001).

[13]S. Auer and D. Frenkel, Phys. Rev. Lett. **91**, 015703 (2003).

[14]S. Auer and D. Frenkel, Annu. Rev. Phys. Chem. **55**, 333–361 (2004).

[15]S. Auer and D. Frenkel, Adv. Polym. Sci. **173**, 149–207 (2005).

[16]D. Winter, P. Virnau, and K. Binder, J. Phys.: Condens. Matter **21**, 464118 (2009).

[17]M. Iwamatsu, J. Chem. Phys. **134**, 234709 (2011).

[18]M. Heni and H. Löwen, J. Phys.: Condens. Matter **13**, 4675–4696 (2001).

[19]H. Wang, H. Gould, and W. Klein, Phys. Rev. E **76**, 031604 (2007).

[20]J. Wang, A. Horsfield, P. D. Lee, and P. Brommer, Phys. Rev. B **82**, 144203 (2010).

[21]L. Farkas, Z. Phys. Chem. **125**, 236–242 (1927).

[22]M. Volmer and A. Weber, Z. Phys. Chem. **119**, 277–301 (1926).

[23]R. Becker and W. Doring, Ann. Phys. **418**, 719–752 (1935).

[24]J. B. Zeldovich, Acta Physicochim. URS **18**, 1–22 (1943).

[25]J. W. Gibbs, *The Collected Works* (Yale University Press, New Haven, 1957), Vol. 1.

[26]B. B. Laird, J. Chem. Phys. **115**, 2887–2888 (2001).

[27]J. Bokeloh, R. E. Rozas, J. Horbach, and G. Wilde, Phys. Rev. Lett. **107**, 145701 (2011).

[28]F. F. Abraham, *Homogeneous Nucleation Theory* (Academic Press, New York, 1974).

[29]D. W. Oxtoby, in *Liquids, Freezing and Phase Transition*, edited by J. P. Hansenan, D. Levesque, and J. Zinn-Justin (Elsevier, Amsterdam, 1991).

[30]D. Kashchiev, *Nucleation: Basic Theory with Applications* (Butterworth Heinemann, Oxford, 2000).

[31]M. Volmer, *Kinetic der Phasenbildung* (Steinkopf, Leipzig, 1939).

[32]D. Turnbull and J. C. Fisher, J. Chem. Phys. **17**, 71–73 (1949).

[33]D. Turnbull, J. Chem. Phys. **18**, 198–203 (1950).

[34]D. Turnbull, J. Appl. Phys. **21**, 1022–1028 (1950).

[35]J. J. Hoyt, J. W. Garvin, E. B. Webb III, and M. Asta, Modell. Simul. Mater. Sci. Eng. **11**, 287–299 (2003).

[36]J. J. Hoyt, Phys. Rev. B **76**, 094102 (2007).

[37]G. Bilalbegovic, F. Ercolessi, and E. Tosatti, Europhys. Lett. **17**, 333–337 (1992).

[38]A. Bolcavage, C. R. Kao, S.-L. Chen, and Y. A. Chang, in *Thermodynamic Calculation of Phase Stability Between Copper and Lead-Indium Solder, Applications of Thermodynamics in Synthesis and Processing of Materials*, edited by P. Nash and B. Sundman (TMS, Warrendale, PA, 1995).

[39]S. Plimpton, J. Comput. Phys. **117**, 1–19 (1995).

[40]W. G. Hoover, Phys. Rev. A **31**, 1695–1697 (1985).

[41]W. H. Press, S. A. Teukolsky, W. T. Vetterling, and B. P. Flannery, *Numerical Recipies in Fortran* (Cambridge University Press, New York, 1992).

[42]R. L. Davidchack and B. B. Laird, J. Chem. Phys. **108**, 9452–9462 (1998).

[43]D. Buta, M. Asta, and J. J. Hoyt, Phys. Rev. E **78**, 031605 (2008).

[44]N. W. Ashcroft and N. D. Mermin, *Solid State Physics* (CBS Publishing, Hong Kong, 1976).

[45]A. P. Thompson, S. J. Plimpton, and W. Mattson, J. Chem. Phys. **131**, 154107:1–6 (2009).

[46]Y. Yang, H. Humadi, D. Buta, B. B. Laird, D. Sun, J. J. Hoyt, and M. D. Asta, Phys. Rev. Lett. **107**, 025505 (2011).

[47]T. W. Barlowh and A. D. J. Haymet, Rev. Sci. Instrum. **66**, 2996–3007 (1995).

[48]A. F. Heneghan, P. W. Wilson, and A. D. J. Haymet, Proc. Natl. Acad. Sci. U. S. A. **99**, 9631–9634 (2002).

[49]A. F. Heneghan and A. D. J. Haymet, J. Chem. Phys. **117**, 5319–5327 (2002).